Chaotic billiards with neutral boundaries

José L. Vega, Turgay Uzer, and Joseph Ford
School of Physics, Georgia Institute of Technology, Atlanta, Georgia 30332-0430
(Received 5 August 1993)

This paper establishes the conditions under which rational billiards, i.e., billiards moving within polygons whose vertex angles are all rational multiples of π, exhibit a chaos that is empirically indistinguishable from that of systems traditionally called chaotic. Specifically, we show empirically that these systems can have positive Liapunov number, positive metric entropy, and positive algorithmic complexity. Although our results appear to contradict rigorous mathematical assertions precluding chaos in rational billiards, such is not the case. In a real sense, rational billiards emphasize the quite practical, physical distinction which exists between continuum and finite mathematics.

PACS number(s): 05.45.+b, 02.60.Cb

I. INTRODUCTION

Chaos is assured in the "diamond" billiard of Fig. 1(a) because of its dispersing boundaries. Chaos continues to occur in the stadium billiard of Fig. 1(b), despite the presence of only neutral and focusing boundaries, because orbits converge toward its separated focal points following which they diverge. Chaos is not to be expected in the polygonal billiard of Fig. 1(c) because its neutral, straight-line segments neither focus nor defocus orbits. These intuitive remarks have a rigorous foundation. The billiards of Figs. 1(a) and 1(b) are known to have positive Liapunov number, positive metric entropy, and positive algorithmic complexity, whereas rational billiards—polygonal billiards whose vertex angles are all rational multiples of π—have null Liapunov numbers, null metric entropy, null algorithmic complexity, plus an isolating integral [1], which restricts system motion on the energy surface. Consequently, rational billiards have historically been categorized as almost integrable [1], pseudointegrable [2], and algorithmically integrable [3]. With these facts in mind, the reader may find it unsettling to notice the striking similarity between the two surfaces of section shown in Fig. 2, one of which corresponds to the chaotic stadium billiard and the other to an "integrable," multisided rational billiard. Moreover, the orbital similarity does not end here. Select any orbit in the stadium and then circumscribe about the stadium a rational polygon [4], whose finite number of sides are tangent to the stadium where sequential orbital boundary collisions occur. This construction makes it apparent that the chaotic stadium billiard and an integrable rational billiard can share the same orbit for as long as one pleases. Surely it is disturbing, if not contradictory, for supposedly integrable and chaotic systems to exhibit such similar behavior. But is this a contradiction easily dismissed by trivial arguments or must we look deeper? As we shall show, these issues can be resolved only by recognizing that the true character of rational billiards has for decades been obscured by the perfections of pure mathematics. This paper seeks to expose the character of rational billiards which emerges when the tenets of continuum mathematics are abandoned.

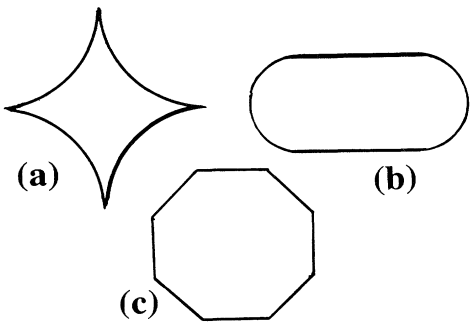

FIG. 1. A billiard moving within the "diamond" shape pictured in (a) above exhibits chaotic motion, as does a billiard moving in the stadium boundary shown in (b). However, a billiard moving within the octagon drawn in (c) is presumed to be ordered and "integrable" in character.

In Sec. II, we review the background required to appreciate the true character of rational billiards, including the fact that they possess closed-form, analytic solutions. In Sec. III, we present numerical results which expose the fact that rational billiards can exhibit an exponentially

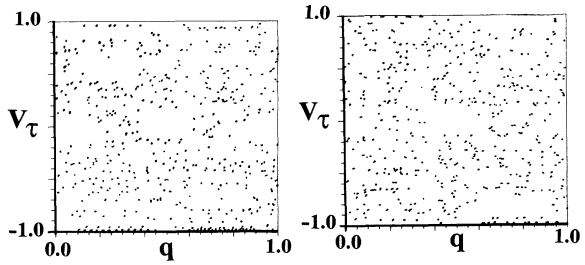

FIG. 2. Shown here are two surfaces of section, one for a billiard moving within a stadium boundary and one for a billiard moving within a multisided polygonal boundary. One system is chaotic the other presumed not. Nonetheless, the similarity is striking. Here, as throughout this paper, V_τ is tangential component of billiard velocity at boundary collision and **q** is distance to the boundary collision point measured along the boundary from a fixed reference on the boundary. (The stadium billiard is on the left.)

sensitive dependence of final state upon initial state despite having the null Liapunov number, entropy, and algorithmic complexity dictated by continuum mathematics. Section IV summarizes our results and discusses the implications they have for physics and mathematics.

II. RATIONAL BILLIARDS

Much of our intuitive understanding regarding the behavior of rational billiards derives from the following three facts: (1) each billiard orbit in position space can be "unfolded" to form a straight line on a plane; (2) each polygon tiles [5] some flat surface under reflection; and (3) some contiguous set of polygons tile the same flat surface under translation. Indeed, these facts provide a route for obtaining an analytic solution for rational billiard motion. Meaning is given to these assertions by examining Fig. 3 for the simple case of a billiard moving in a unit square. Here, an orbit is initiated at the lower left in square 1. Upon striking the boundary, the square is reflected rather than the orbit. This process is repeated at each boundary collision, yielding the dashed line shown. One now observes that the "fundamental square" composed of squares 1, 2, 3, and 4 tiles the plane under translation. These geometric considerations now permit us to write down an analytic expression for the straight-line orbit and then invoke translational periodicity to obtain $X=(X_0+V_{0x}t)$ (mod 2) and $Y=(Y_0+V_{0y}t)$ (mod 2) as the equations for the billiard orbit in the "fundamental square" shown in Fig. 4. Simple geometry [3] then allows us to write down an analytic, closed-form expression for the billiard orbit in square 1. For that small set of polygons which tile the plane under reflection, i.e., those whose interior angles all have the form π/n, the procedures used above for the square are directly applicable. However, the situation is more complicated for polygons

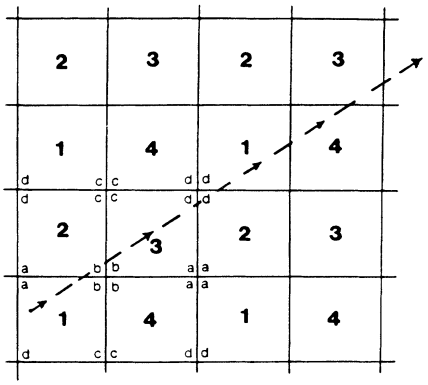

FIG. 3. A billiard orbit in the square is started in the lower left square. At each boundary collision, a square is reflected rather than the orbit. In this way, the billiard orbit is converted into the straight line shown. Indeed all orbits in the square can be represented as straight lines on the plane. This is possible because the square tiles the plane under reflection. The task of obtaining an analytic expression for a billiard orbit in the square is facilitated because squares 1, 2, 3, and 4 tile the plane under translation.

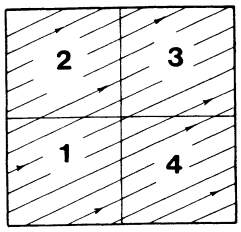

FIG. 4. When all the orbital segments lying in squares 1, 2, 3, and 4 are translated back onto a single 1, 2, 3, and 4 square, the billiard orbit takes the form seen in this figure. Reflecting the orbit back onto a single square now involves only a simple bit of geometry.

having even one interior angle of the form $m\pi/n$, $m>1$. Let us illustrate these complications by considering a particularly simple case—the 60°–120° or $[\pi/3,2\pi/3]$ rhombus shown in Fig. 5(a).

In Fig. 5, we begin to tile a plane by reflecting rhombus 1 into rhombus 2 across side *ab*. Rhombus 2 is then reflected into rhombus 3 as shown. At first glance, it would appear that reflecting rhombus 3 across its side *ab* would yield rhombus 1; however, such is not the case. Upon reflection, the vertices of rhombus 3 do not match those of rhombus 1. This is our first complication; we must abandon the notion of tiling a plane. Nonetheless, we can still proceed by rotating rhombus 3 through 360° into rhombus 4 lying directly under 3. We may now return to reflecting about the $2\pi/3$ vertex obtaining rhombi 5 and 6. Rotating rhombus 6 through 360° finally returns us precisely to rhombus 1. Note that top joins bottom in Fig. 5(d) only at the "gap" represented by the thick line where rhombus 3 connects to 4 and rhombus 6 connects to 1. By unfolding the "double" hexagon of Fig. 5 (d), we

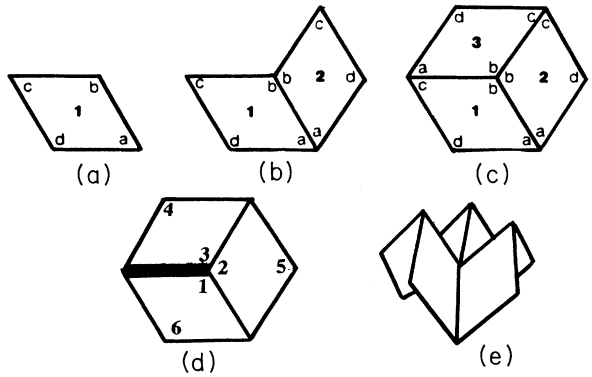

FIG. 5. This figure pictures the beginning of the process which yields the almost everywhere-flat surface upon which the straight-line orbit for a billiard in the 60–120° rhombus may be drawn. Rhombus 1 in (a) is reflected to yield rhombus 2 in (b) and then rhombus 3 in (c). Rhombus 3 is then rotated to obtain rhombus 4 lying directly under 3. Rhombus 4 is reflected to obtain rhombus 5 and thence rhombus 6. The heavy dark line is the "cut" through which rhombus 3 joins rhombus 4 and rhombus 6 joins rhombus 1. If the "double" hexagon of (d) is opened up, one obtains the pleated surface seen in (e). This surface is flat except for the saddle point at its center which carries singular negative curvature.

obtain Fig. 5(e) which exposes a monkey saddle (two valleys for his legs and one valley for his tail) which is flat everywhere except for its central, isolated saddle point which bears singular negative curvature and has the character of a hyperbolic fixed point in the flow [2]. The six connected rhombi of Fig. 5(d), or those in the equivalent Fig. 5(e), form the fundamental set which, under translation, can be used to periodically tile the almost-flat surface upon which straight-line billiard orbits may be drawn. Indeed, translation of the "double" hexagon in Fig. 5(d) yields the everywhere-flat surface (except for the isolated saddle points located at the ends of each thick line segment) shown in Fig. 6, where the flat surface is a "double" plane joined at the upper and lower edges of the narrow "gaps" denoted by the thick line segments—as in Fig. 5(d). As required, this flat surface is tiled under reflection by the rhombus and under translation by the double hexagon. For later reference, we mention that the almost-flat surface periodically tiled under translation by the pleated array of rhombi forming the saddle in Fig. 5(e) is straightforward to construct, but more difficult to draw.

Geometrically, we may draw an orbit for the rhombus billiard as a straight line on this flat surface and regain the orbit in the rhombus by repeated reflections, just as in the case of the square. Analytically, however, we encounter a second complication. A glance at the straight-line billiard orbit drawn in Fig. 5 immediately reveals the problem. Please note that the zigzag look of this straight line geodesic arises because it lies on two connected planes rather than just one. Here, it is visually apparent that the correct analytic expression for the full rhombus orbit is not simply $X=X_0+V_{0x}t$, $Y=Y_0+V_{0y}t$, as it was for the square. Nonetheless, once the X-Y axes are chosen for each plane, the standard equation for straight-line segments can be used on each plane. Thus, to keep proper track of the complete straight-line rhombus orbit, we must maintain a record of the sequential "planes" upon which each straight-line segment lies,

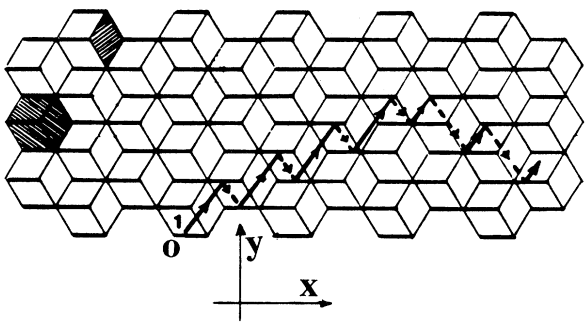

FIG. 6. The almost everywhere flat surface upon which the straight line 60°–120° rhombus orbits may be drawn. It is obtained by translating the "double" hexagon of Fig. 5(d). This surface consists of two planes joined at the upper and lower edges of each heavy line. Singular points of negative curvature exist at the ends of each heavy line. The zigzag curve is actually a straight line geodesic on this flat surface. The continuous segments lie on the "top" plane while the dotted segments are on the "bottom."

or better, develop an analytic expression for the transition of the orbit from plane to plane. For the case at hand, the 60°–120° rhombus, Eckhardt, Ford, and Vivaldi [3] established that the plane-to-plane transitions could be encoded as a closed-form (mod 3) function whose detailed form need not concern us here. Once this fact was established, gaining a closed-form analytic solution for rhombus orbits was no more difficult than for the square. Finally, the closed-form solution thus derived was shown to logarithmically compress the information in the rhombus orbits, just as does the solution for the square.

In the general case, we can construct the everywhere-flat surface (except at isolated saddle points which add a hyperbolic character to the flow) simply by continuing indefinitely and in all directions the process of "rotating" each polygon about each vertex until each time the polygon returns to its initial configuration. It helps to understand the construction envisioned here if, for the simplest case, one cuts out a large number of paper rhombi and continues the saddle-point figure of Fig. 5(e) by sequentially scotch taping six rhombi about each vertex. This "hands on" construction quickly reveals that the isolated saddle points embedded in this almost-flat surface provide it with average negative curvature. In any event, once the reflection process is completed for an arbitrary rational polygon, one has an almost everywhere-flat surface which is tiled under reflection by the given polygon and under translation by some finite set of the polygons [1–3]. As before, each saddle point is the junction of a number of planes (2π regions). Again, one must determine a closed-form expression for the transition of the straight-line polygon billiard orbit from one plane to the next. Although an explicit expression for these transitions has not yet been derived for an arbitrary polygon, the derivation for any specific polygon requires only that we track the billiard orbits and keep a record of where they go. However, since we have no need of exact solutions in this paper, we shall not pursue this issue further here.

Much more important for us is the fact that, in general, the orbits of rational billiards lie on almost everywhere-flat surfaces which, nonetheless, have average negative curvature, a widely accepted signature of chaos. Moreover, the average density of the isolated, singular points bearing the negative curvature grows as the number of polygonal sides increases. Now, average negative curvature connotes rapid separation of initially parallel, close orbit pairs. But how can polygons with neutral boundaries disperse parallel orbits? Of course, the neutral boundaries cannot, but the singular vertices ($m\pi/n$, $m>1$) can. A particularly striking example is shown in Fig. 7 which pictures the dispersion of two incoming, parallel orbits by a $3\pi/2$ vertex. This figure makes it quite clear that the future history of a polygonal orbit crucially depends on the side it takes in passing a singular vertex. However, when a polygonal boundary has only a few such vertices, dispersion might be expected to play only a relatively minor role in the overall motion. But as the number of vertices increases, dispersive effects may become hard to ignore. In the following section, we verify that this is indeed the case.

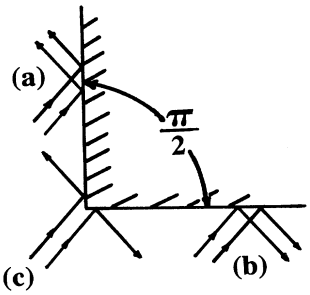

FIG. 7. Three close parallel orbit pairs incident on the sides of a singular $3\pi/2$ vertex. At (a) and (b) both members of each pair strike the boundary on the same side of the vertex and emerge parallel after the collision, while at (c) the two members of the pair fall upon opposite sides of the vertex and emerge antiparallel. This is an especially striking example of orbital dispersion due to singular vertices.

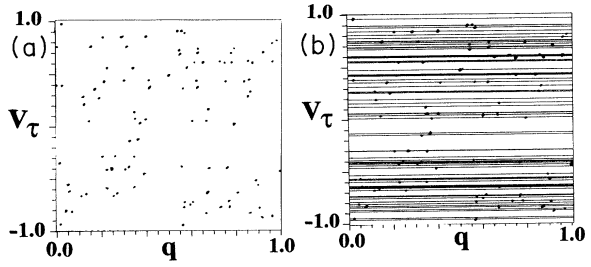

FIG. 8. The surface-of-section points for a single stadium orbit are shown on the left. Over the time interval considered this stadium orbit is the same as that of a judiciously chosen, circumscribed rational polygon, which latter has an isolating constant of the motion that limits the number of allowed V_τ values. At the right, it is shown that the stadium surface of section points lie precisely on these allowed V_τ lines and nowhere else. In short, there is a hidden order in the short-term stadium motion.

III. NUMERICAL RESULTS

The surfaces of section shown in Fig. 2 certainly reveal the erratic character of orbits for the stadium and the associated circumscribed, multisided polygon. However, surfaces of section are not a strong test for chaos. Indeed, they do not distinguish chaos from simple ergodicity nor do they permit one to rule out the presence of a subtle order. For example, in Fig. 8(a) we show surface-of-section points generated by a single stadium orbit. To expose its hidden order, we used the technique described in our opening section to circumscribe a rational polygon about this stadium such that the polygon and the stadium share the orbit generating the points shown in Fig. 8(a). Recall now [3] that billiard motion in a rational polygon has only a finite number of velocities, and, because the stadium and polygon here share the same orbital segment, this means that there can be only a finite number of values for V_τ in the stadium surface of section shown in Fig. 8(a). Hence, we analytically computed these V_τ values [1], and in the comparison Fig. 8(b), we reveal that all the stadium surface-of-section points in Fig. 8(a) do, in fact, lie on predictable horizontal V_τ lines and nowhere else. Thus, we have exposed a hidden order in the chaotic motion of a stadium. However, this order is detectable only over a short-time interval. A polygon can share an orbit with a stadium over an extended period only if the polygon has an enormous number of sides. The corresponding set of V_τ values would then be so dense they would appear to form a continuum. Having now verified that a surface of section is not a trustworthy test for chaos, let us turn to one that is.

Liapunov number is widely regarded as the definitive test for chaos since, when positive, it implies an exponential sensitivity of the final state to variation in the initial state. Thus, putting caution aside, we elected to compute the Liapunov number numerically for a sequence of polygons having an increasing number of sides, all circumscribed about the same stadium. The results are shown in Fig. 9. For side number $N \geq 1000$, the empirical Liapunov number for the polygons takes on a constant value equal to that of the stadium. The numerical procedures used here closely followed those presented by Benettin and Strelcyn [6]. Specifically, each member of a Liapunov orbit pair—consisting of a reference and a comparison orbit—was started at the same spatial position with initial velocity directions separated by an angular distance $\alpha = 10^{-3}$ rad. Each member of the orbit pair was then permitted to evolve with time. Periodically, however, the state of the comparison orbit was reinitialized. Specifically, let d_0 be the magnitude of the initial phase-space separation distance between comparison and reference orbits, and let $\mathbf{D}$ be the time-evolved vector phase-space distance at the moment of reinitialization. The comparison state is then moved along the vector $\mathbf{D}$ until it reaches the point $d_0\mathbf{D}/|\mathbf{D}|$. The magnitude of separation distance between comparison and reference orbit is thus returned to its initial value but its direction is not necessarily the same. We then compute the Liapunov number λ using the Benettin-Strelcyn formula $\lambda = (1/n\epsilon)\sum_{i=1}^{n} \ln(|\mathbf{D}_i|/d_0)$, where ϵ is the reinitializa-

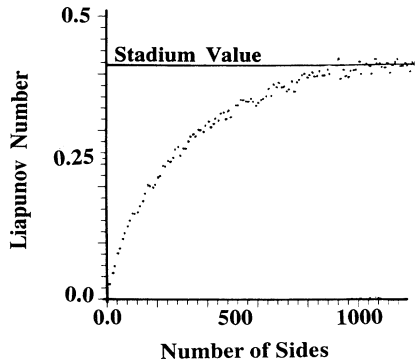

FIG. 9. Liapunov number of polygons circumscribed about the same stadium. Each point in the figure represents the Liapunov number averaged over numerous orbit pairs at each value N of side number. The polygonal values of the Liapunov number stabilize and take on the Liapunov number of the stadium at about side number $N = 1000$.

tion period and n is the number of such periods. The Liapunov numbers we computed for the stadium were the same as those reported by Benettin and Strelcyn. Each point plotted in Fig. 9 is an average of the Liapunov numbers computed for numerous orbit pairs at each N value. Each orbit pair was integrated until it gave a stationary value for Liapunov number. The fact that the polygonal Liapunov numbers become equal to that of the stadium should not be permitted to overshadow the fact that polygons having only a few sides exhibit a positive, albeit small, Liapunov number.

At this point, one is tempted to conjecture that the results shown in Fig. 9 are merely a consequence of our considering only polygons circumscribed about a chaotic system—here the stadium. Put simply, as the polygonal shape approaches that of the stadium, so presumably does its orbital behavior. Bearing this thought in mind, let us inspect Fig. 10 which presents a plot of numerically computed Liapunov number versus the side number N for polygons circumscribed about an integrable system—the circle. Here, the Liapunov number achieves a constant value for $N \geq 200$, and moreover this constant value is not the same as that shown in Fig. 9. To corroborate this Liapunov result, in Fig. 11 we show the linear growth of separation distance between two circle orbits pictured just above the exponential separation of two orbits in a circumscribed polygon. Finally, recall that L_z and, hence, V_τ, is a constant of the motion for the circle billiard; therefore, each orbit for the circle must lie on a single horizontal line in a surface of section plot. Again bearing this thought in mind, glance at Fig. 12 showing a composite of surfaces of section for a circumscribed polygonal billiard. In Fig. 12(a), surface-of-section points spread rapidly along the constant V_τ "direction" but more slowly along the direction perpendicular to constant V_τ. The continuing spread in V_τ values is shown in Figs. 12(b) and 12(c). This behavior is reminiscent of that

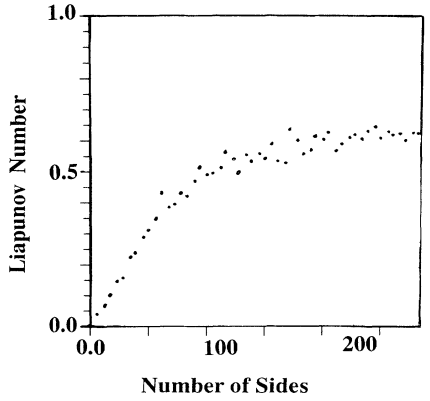

FIG. 10. Liapunov number for polygons circumscribed about the same circle. A positive Liapunov number is obtained despite the fact that polygonal shape approaches more and more closely to that of the integrable circle as polygonal side number increases. Polygonal Liapunov number achieves and maintains a constant value distinct from that seen in Fig. 9, moreover, saturation occurs at a much lower value of side number.

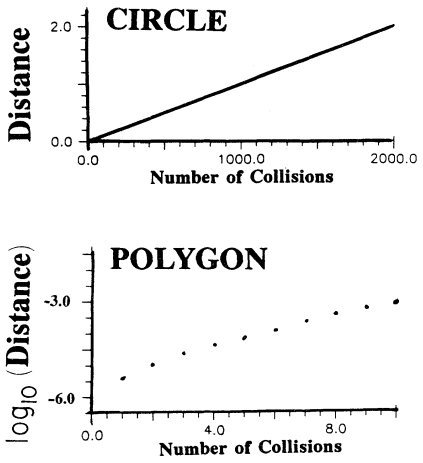

FIG. 11. This figure compares the linear growth of separation distance for close orbit pairs in the circle with the exponential separation of close orbit pairs in a circumscribed polygon.

exhibited by Chirikov's kicked rotor [7]. In closing this paragraph, we can but note that, while a circumscribed billiard is not ignorant of the behavior of the billiard about which it is circumscribed, it nonetheless superimposes its own "brand" of chaos. Specifically, the polygonal boundary contains singular points whereas the enclosed smooth boundary does not.

Let us now begin to reconcile the rigorously derived null Liapunov number, entropy, and algorithmic complexity of rational billiards with the numerical results of Figs. 9–12. In Fig. 13, we compare our analytical estimate with empirical data regarding the number of polygonal sides required to obtain a meaningful (nonzero) Liapunov number versus initial velocity angular separation α. The curve in Fig. 13 represents our crude esti-

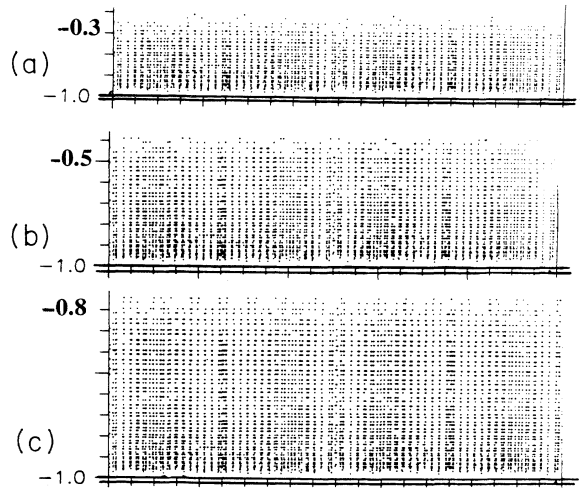

FIG. 12. Three surfaces of section in the $(V_\tau, \mathbf{q})$ plane for a polygon circumscribed about a circle. Here, the total orbital integration time increases from (a) to (b) to (c), and one notes that the spread of polygonal points in the vertical V_τ direction is increasing. For comparison, recall that V_τ is a constant of the motion for the circle billiard.

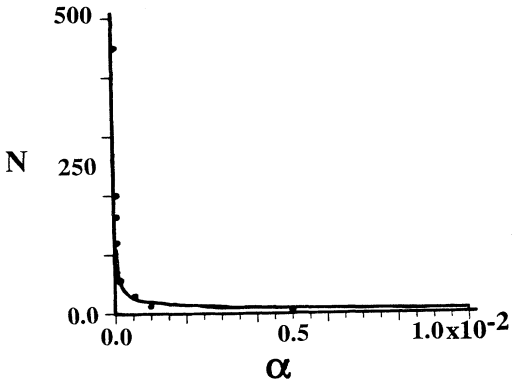

FIG. 13. The smooth curve is a plot of $N=C/\sqrt{\alpha}$, our rough estimate of when Liapunov orbit pairs will clearly perceive the average negative curvature of the almost everywhere-flat surface upon which the polygonal billiard orbits move. Here, of course, N denotes the number of polygonal sides and α is the initial angle between velocity directions for a Liapunov pair. The dots in the figure are the empirical values of N, for given α, at which a stable, nonzero value of Liapunov number was first observed.

mate, $N=C/\sqrt{\alpha}$, while the dots are numerically computed data points. The meaning of this figure reads as follows. For a given N, an α value must be large enough for the Liapunov pair to be fully affected by the negative curvature of the almost everywhere-flat surface. As the value of α decreases toward zero, Liapunov orbit pairs increasingly are affected by more and more of only the flat surface, and for $\alpha\approx 0$ report back the null Liapunov number required by continuum mathematics. However, if one fixes the value of $\alpha>0$, no matter how small, there is nonetheless a value of N beyond which a positive value of the Liapunov number will be obtained. In this regard, it is to be emphasized that this empirical Liapunov number for rational polygons achieves a constant value (saturates) with time, with α, and with N as is shown below.

Figure 14 demonstrates that Liapunov number

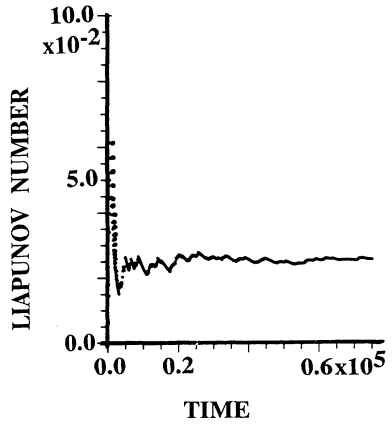

FIG. 14. This figure is intended to provide empirical evidence that, once a steady value of the Liapunov number is achieved by an orbital pair, this constant value is maintained throughout all time. This graph is for a polygon having 22 sides using $\alpha=10^{-3}$.

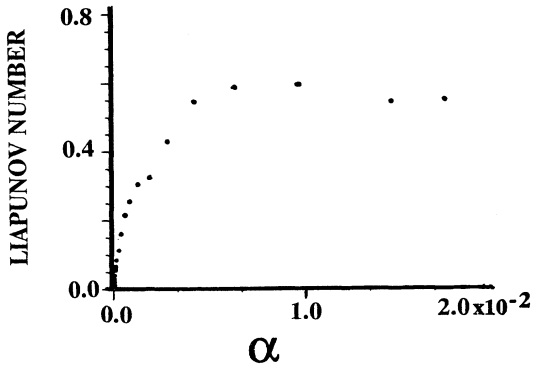

FIG. 15. This figure reveals that a Liapunov number saturates with increasing α at fixed side number N. It corroborates the notion that, once α permits a Liapunov pair to perceive the average negative curvature of the almost everywhere-flat surface, the Liapunov number stabilizes and does not increase indefinitely with α.

achieves and maintains a constant value over quite long-time intervals. The small value of the Liapunov number observed here was obtained for a polygon having 22 sides using $\alpha=10^{-3}$. This result should by now come as no surprise. If α is large enough for an orbit pair to be affected by the negative curvature of the almost-flat surface at time zero, then the homogeneity of that surface will permit the pair to be affected by that negative curvature forever. Figure 15 illustrates the saturation of Liapunov number with α while Fig. 16 presents a more complete picture of saturation with N than given by the earlier Fig. 9.

Saturation with N at fixed α is a bit surprising, especially in view of the widely held notion that the similarity of boundary implies similarity of motion. It therefore deserves an explanation. As the polygonal boundary

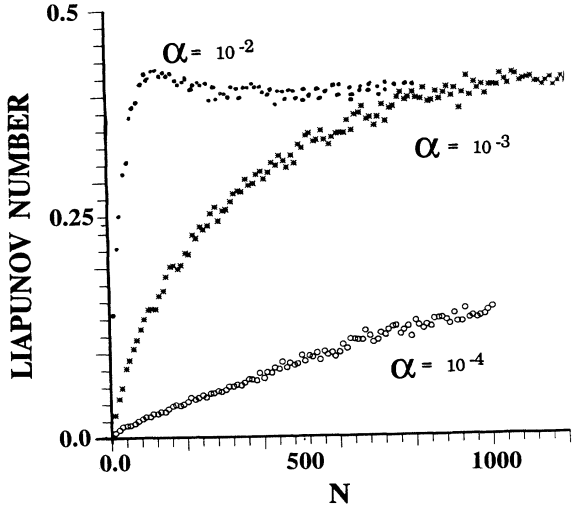

FIG. 16. This graph is a continuation of Fig. 9 and plots the Liapunov number versus N for polygons circumscribed about a stadium for three values of α. This figure exposes the saturation of the Liapunov number with both N and α.

grows close to the enclosed curve, the angle between adjacent sides tends to π. In short, the dispersion due to a single vertex tends to zero. However, as N increases at fixed α, the separation between the two orbits of a Liapunov pair spans not one but many vertices. Simple geometry then shows that the product of increasing N and decreasing "scattering" per vertex is a constant. Consequently, the same value of Liapunov number is observed no matter how large the finite value of N.

Thus far, we have emphasized Liapunov number and not metric entropy or algorithmic complexity. We rectify this omission in the following section.

IV. CONCLUSIONS

Continuum mathematics quite correctly asserts that all rational billiards have null Liapunov number, entropy, and algorithmic complexity. However, these assertions are based on assumptions that we frequently overlook or ignore, assumptions we may not wish to accept or cannot accept. All three of these notions [8] invoke the limit $t \to \infty$, and all require that system orbits be known with infinite precision. In addition, the Liapunov number requires arbitrarily close initial orbit pairs; entropy requires phase-space partitions having arbitrarily small cell size; and algorithmic complexity requires that N^{ϵ} be distinguishable from N, no matter how close ϵ is to 1.

The common thread linking the above assumptions is infinite accuracy. Invoking the postulate that nothing, in principle, prevents the measurement of any quantity to arbitrarily high precision, physical scientists adopt the mathematical notion of infinite accuracy without demur, notwithstanding the fact that all laboratory observations and computer calculations have finite accuracy. However, the physical data have, in fact, so frequently fit the continuum theory that the scientist feels no compelling need to incorporate the subtleties of finite mathematics.

However, rational billiards offer at least a small reason to rethink this position, for if we have only finite accuracy, no matter how high, there exist rational billiards which empirically possess positive Liapunov number, entropy, and algorithmic complexity. The reasons for the positive Liapunov number have already been given. These systems have positive entropy because the cell size cannot go to zero and because the positive Liapunov number ensures that the average information gained per measurement is not zero. Turning now to algorithmic complexity, let us seek to compute sequential orbital points all having a finite accuracy less than the maximum available. For sufficiently large N, each time this orbit reaches the boundary, it strikes a vertex "head on." In order to resolve the crisis, we continue the orbit to the right or left of the given vertex as the center of the orbit's "error bar" lies to the right or left of the vertex. For long orbital segments, the information put in to compute the straight-line segments grows like $\log_{10} t$ but the information in the binary decisions required to resolve the sequential crises grows like t. The full orbit, therefore, has positive complexity. There is an analogy here to a Galton board. If both ball and pins are mathematical points, the ball descends rarely encountering a pin. However, if the ball has a finite diameter and the pins are suitably numerous, the path of the ball is a random walk. In summary, if only finite precision is available (no matter how high), the chaos displayed by rational billiards is indistinguishable from that exhibited by systems traditionally termed chaotic.

Using arguments based on continuum mathematics, mathematician and physicist alike have concluded that rational billiards are integrable—almost integrable, pseudointegrable, or algorithmically integrable. However, by restricting ourselves to finite mathematics, we have shown in this paper that the overwhelming majority of rational billiards are, in fact, chaotic [9].

[1] A. N. Zemlyakov and A. B. Katok, Math Notes **18**, 760 (1976); **20**, 1051 (1976).

[2] P. J. Richens and M. V. Berry, Physica D **2**, 495 (1981).

[3] B. Eckhardt, J. Ford, and F. Vivaldi, Physica D **13**, 329 (1984).

[4] If the polygon thus constructed has one or more vertex angles which are not rational multiples of π, they can be made so by negligible changes since the rational angles are dense.

[5] The world "tile" here means that the relevant surface is covered by the specified objects without gaps or overlap.

[6] G. Benettin and J.-M. Strelcyn, Phys. Rev. A **17**, 773 (1978).

[7] G. Casati, B. V. Chirikov, F. M. Izraelev, and J. Ford, in *Stochastic Behavior in Classical and Quantum Hamiltonian Systems*, edited by G. Casati and J. Ford, Springer Lecture Notes in Physics Vol. 93 (Springer-Verlag, Berlin, 1979).

[8] Actually, algorithmic complexity applies equally well to both finite and infinite objects. However, we have here spoken of "null complexity," a technical term which implies the limit $t \to \infty$.

[9] Indeed, after completing the work described herein, we discovered a paper by T. Cheon and T. D. Cohen, Phys. Rev. Lett. **62**, 2769 (1989) which foresaw the possibility of our results.